

Wave observations from an array of directional buoys over the southern Brazilian coast

Henrique Patricio Prado Pereira¹  · Nelson Violante-Carvalho¹ ·
Izabel Christina Martins Nogueira¹ · Alexander Babanin² · Qingxiang Liu² ·
Uggo Ferreira de Pinho¹ · Fabio Nascimento¹ · Carlos Eduardo Parente¹

Received: 14 June 2017 / Accepted: 12 October 2017 / Published online: 25 October 2017
© Springer-Verlag GmbH Germany 2017

Abstract It is well known that the majority of buoy measurements are located around the US coast and along some European countries. The lack of long-term and densely spaced in situ measurements in the Southern Hemisphere in general, and the South Atlantic in particular, hinders several investigations due to the lack of detailed metocean information. Here, we present an effort to overcome this limitation, with a dense network of buoys along the Brazilian coast, equipped with several meteorological and oceanographic sensors. Out of ten currently operational buoys, three are employed to present the main characteristics of waves in the Southern part of the network. For the first time, sensor characteristics and settings are described, as well as the methods applied to the raw wave data. Statistics and distributions of wave parameters, swell propagating events, comparison with a numerical model and altimeters and a discussion about the occurrence of freak waves are presented.

Keywords Wind-waves · Buoy network · South Atlantic

1 Introduction

The lack of in situ measurements in the Southern Hemisphere is well known, and the South Atlantic (SA) is no

exception (Hemer et al. 2009; Chawla et al. 2013; Rapizo et al. 2015; Souza and Parente 1988; Cuchiara et al. 2009; Pianca et al. 2010). More specifically, studies based on wave measurements over the Brazilian coast are up to the present spatially sparse, limited mainly to its most important oil fields, located in Campos Basin (Violante-Carvalho et al. 2004). The shortage of in situ wave data in this region has resulted in numerical modelling becoming the most widely used tool for the investigation of its wave climate (Parise and Farina 2012). Comprising around 7.5 thousand kilometres, the Brazilian coastline is the longest in the SA, consequently of prime importance for its characterization.

Most of the wave buoys under supervision of the National Oceanic and Atmospheric Administration (NOAA) are located in mid-latitudes in the Northern Hemisphere mainly in relatively shallow waters. The other major source of directional wave data is the network deployed along the coasts of Western Europe, as well in comparatively shallow waters. The majority of the Brazilian coast is located in the tropical zone, being strongly affected by swell all year round and therefore with most of the energy in the low frequency portion of the spectrum (Violante-Carvalho et al. 2004). Multi-modal spectra is another common feature in the southernmost part of the Brazilian coast, with in average only one fourth of the cases classified as unimodal (Violante-Carvalho et al. 2004). The availability of in situ data with such characteristics, multi-modal spectra with the presence of a swell component all year round, is very scarce.

In an attempt to overcome the lack of in situ measurements, Brazil's PNBOIA (National Buoys Program) was launched in April 1997 along with the pilot program GOOS (Global Ocean Observing System-Brazil). The goals of this program encompass the collection of metocean data in the Atlantic Ocean along the Brazilian coast, by means of a network of moored buoys and drifters supporting

Responsible Editor: Bruno Castelle

✉ Henrique Patricio Prado Pereira
henriqueppp@oceanica.ufrj.br

¹ Ocean Engineering Program, Federal University of Rio de Janeiro, Rio de Janeiro, Brazil

² Department of Infrastructure Engineering, University of Melbourne, Melbourne, Australia

meteorological and oceanographic activities important to public institutions and companies. Coordinated by the Brazilian Navy, the program involves the collaboration of public universities, PETROBRAS (the Brazilian Oil Company) and public research institutions. It is PNBOIA's intention to install a monitoring program with a total of ten moored buoys (Fig. 1, zoom out and Table 1), with historical data freely downloadable at <http://www.goosbrasil.org>.

Here, the focus will be mainly in the three southernmost buoys which have simultaneous measurements, named Rio Grande/RS (RIG), Florianopolis/SC (FLN) and Santos/SP (SAN) (Fig. 1, zoom in), approximately 400 km apart, spanning a distance of over one thousand kilometers. These buoys were deployed on the edge of the continental shelf, at a depth of approximately 200 m and roughly aligned along the great circle along which swells propagate in the region, in a nearly southwest-northeast direction.

The current dataset is particularly interesting because of the lack of consistent and available measurements in the subtropical zone of the SA, which have distinct typical values of for instance wave age and wave slope when compared to higher latitudes of the northern hemisphere, where in general most in situ acquisitions are conducted. The characteristics of the wind waves are key in the air-sea interface exchanges and in the modulation of the lower atmosphere (Badulin et al. 2007). Therefore, the subtropics with their particular wind forcing and energy ratio between high and low frequency bands are an interesting area to investigate wave generation, propagation and attenuation. It is worth noting that the few previous studies published about the SA

were either based on numerical modelling or referred to a single location. This paper presents wave characteristics for the Brazilian southern offshore region, based on a five month series (February/2012–June/2012) where wave data was simultaneously measured by three directional buoys without significant gaps.

The paper is organized as follows. In Section 2, sensor characteristics and settings are described, as well as the methods applied to the raw wave data. Statistics and distributions of the wave parameters are presented and discussed in Section 3.1. Some events of swell propagating along the three aligned buoys were recorded and in Section 3.2 we describe one of them in terms of its spectral evolution. A comparison between the in situ data and a wave hindcast from WAVEWATCH III (WW3) numerical model is presented in Section 3.3, employing two distinct source terms. A comparison against radar altimeters is made in Section 3.4. Another interesting feature of this dataset is that some sea states present a value of the ratio H_{max}/H_s higher than 2, which are related to freak waves, considering the criteria normally encountered in the literature (Liu 2007; Kharif and Pelinovsky 2003). They are discussed in Section 3.5.

2 Methods

In Table 1, the location (city/state), position, distance to shore (DS) and depth (DP) of the ten buoys are listed. With the exception of the two buoys in the state of Rio de Janeiro

Fig. 1 Location of the ten oceanic buoys (on the top left) and a zoom on the three southernmost ones (on the right). The larger area (on the top left) coincides with Grid 1 employed in the wave model, while the one in detail is the same as Grid 2 (see Table 4 for more information). The circle represents the position of Campos Basin

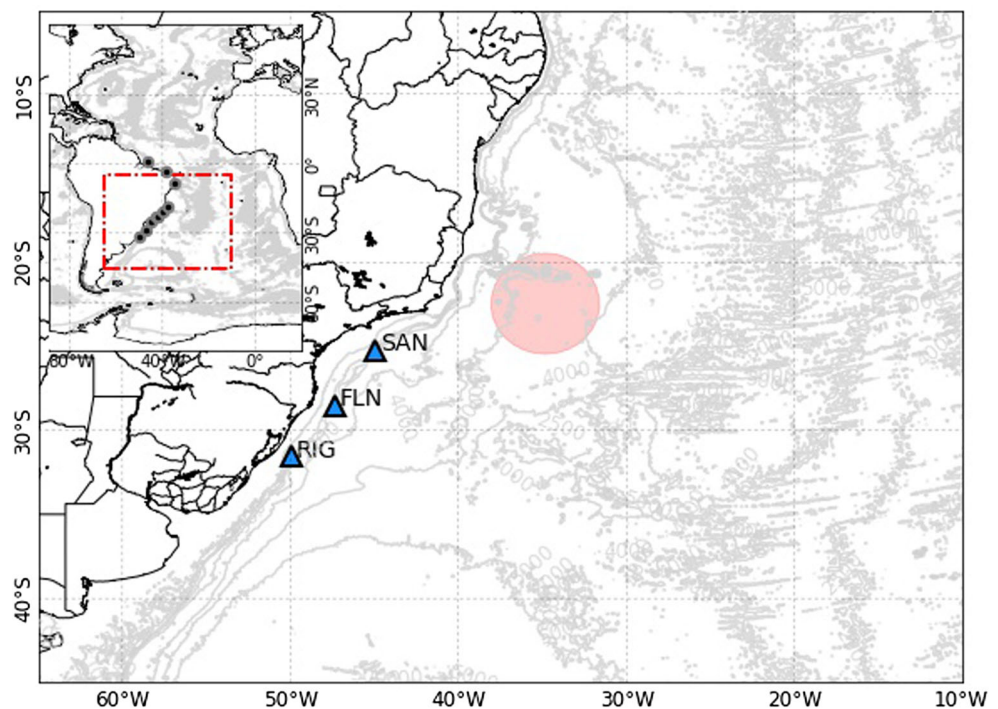


Table 1 Buoy’s location, distance to shore (DS) and depth (DP) of the ten PNBOIA’s buoys

Buoy’s location	Lat/Lon	DS (km)	DP (m)
Barra Norte/AM	01.094/−46.350	307	200
Fortaleza/CE	−02.987/−38.819	61	200
Recife/PE	−08.149/−34.560	34	200
Porto Seguro/BA	−18.151/−37.944	150	200
Vitória/ES	−20.278/−39.727	41	200
Cabo Frio/RJ	−22.995/−42.187	5.7	60
B. Guanabara/RJ	−22.924/−43.150	1.8	25
Santos/SP	−25.283/−44.933	180	200
Florianopolis/SC	−28.500/−47.366	130	200
Rio Grande/RS	−31.566/−49.966	100	200

(Baia de Guanabara and Cabo Frio, deployed at 25 and 60 m deep, respectively), the others are located at the edge of the continental shelf, at the 200 m isobath.

Most of PNBOIA’s buoys were developed by AXYS Technology with a 3 m diameter hull (Axys-3M). This type of buoy is able to provide directional wave information using the directional wave sensor TriaxisTM, which is equipped with three accelerometers and three angular sensors that enable to measure vertical and horizontal accelerations, as well as heave, pitch and roll movements. Raw data are pre-processed in the buoy’s internal module and sent via satellite. Only wave parameters such as significant wave height (Hs), maximum wave height (Hmax), peak period (Tp) and peak direction (Dp) are sent to inland servers. The direction represents where the waves comes from. The raw wave data (spectra and time series) are stored in the buoy’s internal memory and retrieved during periodical maintenance. Besides providing wave information, this type of buoy also measures meteorological parameters and ocean current profiles.

The buoys are equipped with two anemometers, located at 3.7 and 4.7 m above sea level. The measured data can be corrected to the 10 m height according to the methodology described by Liu et al. (1979). Wind gust is represented by the average of the five highest values of wind velocity during the sampling period. Relative air humidity is measured together with air temperature and dew point by means of a hygrothermograph. A pyranometer is used to measure the solar radiation. Each PNBOIA’s buoy has a 400 kHz ADCP (Acoustic Doppler Current Profiler) mounted 0.5 m below the water level, looking downwards. This configuration allows the measurement of ocean currents in 20 layers of 2.5 m thickness each with a blanking distance of 5 m. This way it is possible to obtain current data down to almost 60 m. The ADCP has a built in thermometer that is used to measure the sea temperature at 0.5 m depth. Table 2 lists the most common settings of the sensors.

Table 2 Most common settings of the sensors used in the metocean buoys

Parameter	Samp. Freq.	Samp. time
Wind direction	1 Hz	10 min
Wind intensity	1 Hz	10 min
Wind gust	1 Hz	5 s
Air temperature	1 Hz	10 min
SST	1 Hz	10 min
Atmospheric Pressure	1 Hz	10 min
Relative air humidity	1 Hz	10 min
Dew point	1 Hz	10 min
Solar radiation	1 Hz	10 min
Wave height	1.28 Hz	17 min
Wave period	1.28 Hz	17 min
Wave spectrum	1.28 Hz	17 min
Wave direction	1.28 Hz	17 min
Current velocity	1 Hz	20 min

Wave data analysis was performed both in the time and frequency domain. In time domain, each individual wave was selected using the zero-crossing method and then the significant wave height (Hs) and maximum wave height (Hmax) were computed. Three time series were used to perform the spectral analysis, the vertical displacement $\eta_1(t)$ and $\eta_2(t)$, and $\eta_3(t)$, the east-west and north-south displacements, respectively. Sampling intervals with a length of 17 min were taken each hour with a sampling rate of 1.28 Hz. The spectral estimators were obtained using the Welch method (Welch 1967) employing a Hanning window and 50% overlap between adjacent segments. Records consisting of 1312 data points were segmented into 4 partitions of 328 points yielding 14 degrees of freedom and a frequency resolution of 0.0039 Hz. Wave spectral parameters, such as the zero-moment wave height (Hm0) and the peak period (Tp) are obtained from the wave spectra. The first two Fourier coefficients (a_1 and b_1) are calculated from the co- and quadrature spectra (Tucker and Pitt 2001) and the mean wave direction (θ_p) corresponding to the peak frequency (f_p) is obtained according to the following:

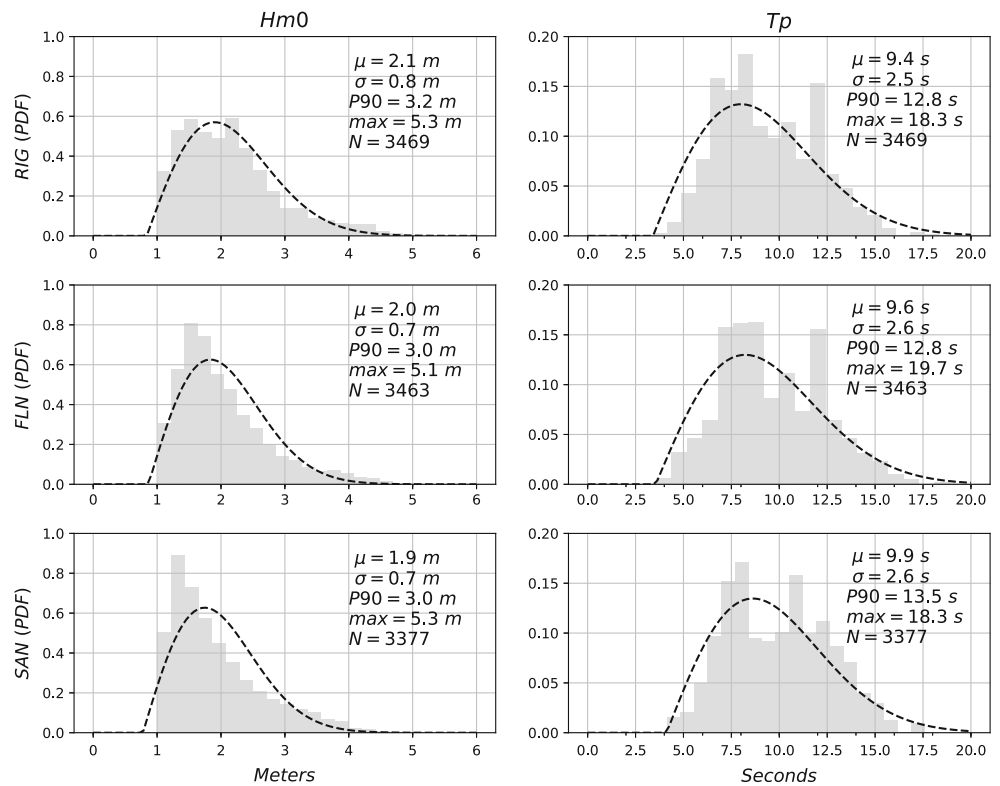
$$\theta_p = \arctan \left[\frac{b_1(f_p)}{a_1(f_p)} \right] \tag{1}$$

3 Results

3.1 Wave parameters statistics

The statistical analysis aims to describe the general wave parameters for each one of the three aligned buoys. Histograms of the main wave parameters, tables with mean and

Fig. 2 Zero-moment wave height ($Hm0$) on the left panels and peak period (Tp) on the right panels. Probability Distribution Functions (PDF) for the five months of analysis and the Rayleigh distribution (dashed lines). Mean (μ), standard deviation (σ), 90th percentile ($P90$), maximum (max) and number of data points (N) are also presented



maximum values and joint distributions are given. The wave analysis was made both in time and frequency domain.

Normalized distributions of the zero-moment wave height ($Hm0$) and peak period (Tp) are shown in Fig. 2, as well as Rayleigh and normal curves for comparison with $Hm0$ (left panel) and Tp (right panel), respectively. On the right panel, two maxima of peak period are discernible. One is representative of wind-sea with 6 to 8 s and the other representative of swell with approximately 12 s.

Table 3 shows that the mean $Hm0$ values decrease from south to north, inversely to what happens to the mean Tp

values. The mean peak direction (Dp) values are mainly from SE, but it is important to keep in mind the bimodal characteristics of waves in this region, with predominant winds (and consequently the high frequency waves) from NE. In the southern Brazilian coast, the swell generally comes from the S/SW and wind-sea varies from NE under the influence of the South Atlantic Anticyclone (SAA) and from S/SE to S/SW in the presence of extratropical cyclones. The maximum significant wave height ($Hm0$), registered for the three buoys, shown in Table 3, represents the same event, in June 2012. For the Rio Grande buoy,

Table 3 Mean values for $Hm0$, Tp and Dp for the three buoys (above dashed line) and absolute maximum significant wave height ($max. Hm0$) values attained during the sampling period (below dashed line)

Wave Param.	RIG	FLN	SAN
$\overline{Hm0}$ (m)	2.1	2.0	1.9
\overline{Tp} (s)	9.4	9.6	9.9
\overline{Dp} (°)	133	138	142
N° of points	3469	3463	3377
<i>Date max. Hm0</i>	2012/06/09 07 h	2012/06/07 11 h	2012/06/10 01 h
$Hm0$ (m)	5.3	5.1	5.3
$Hmax$ (m)	7.8	7.6	7.4
Tp (s)	13.5	9.9	14.2
Dp (°)	181	214	185

Dates of the occurrence of maximum $Hm0$ recorded, as well as $Hmax$, Tp and Dp values associated with the sea state during which the maximum $Hm0$ took place are also shown

Hm0 reached 5.3 m on 2012/06/09 at 07 h. Two days before, the Florianopolis buoy measured 5.1 m and then the Santos buoy measured 5.3 m one day after. The maximum wave height (Hmax) related to this event was 7.8, 7.6 and 7.4 m for Rio Grande, Florianopolis and Santos, respectively, with Tp values of 13.5, 9.9 and 14.3 s and Dp of S, SW and S. The periods related to the maximum wave height (THmax, estimated with the zero upward crossing method) were 14.8 s for Rio Grande, 10.1 s for Florianopolis and 14.0 for Santos. The average values of the main wave parameters were similar in all of the three buoys, with values of Hm0, Tp and Dp close to 2.0 m, 9.6 s and 137°, respectively.

Wave height and wave period roses (Fig. 3) show that the main wave directions on Rio Grande are from S/SW with wave heights up to about 4.5 m and periods over 16 s. Florianopolis' wave heights present values as high as 4.5 m but with a lower percentage of occurrences than that of Rio Grande's and maximum wave period values reaching up to 18 s. Santos buoy recorded waves with short periods coming from E/NE and with a higher occurrence of long period waves from S. In Florianopolis, there is still a clear dominance from southerly and northeasterly waves, although the waves are more evenly distributed than in Rio Grande.

In order to assess the distributions of surface elevation at the three buoys, located in relatively deep waters, and to compare with normal distributions, all time series were

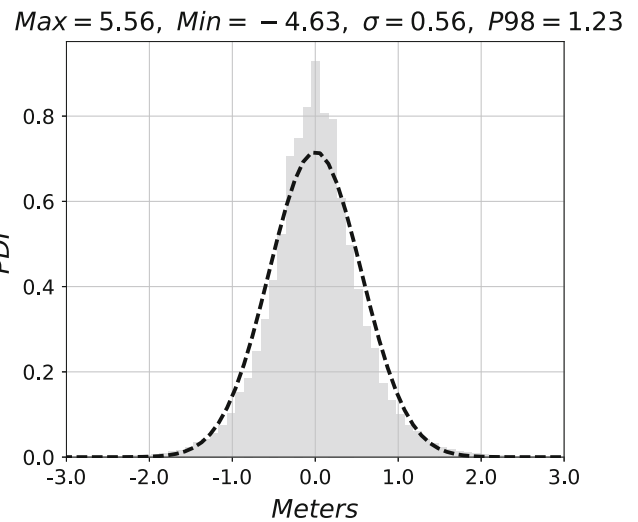


Fig. 4 Heave values distribution. Comparison with normal distribution (dashed line). σ is the standard deviation and P98 is the 98th percentile

united to plot the histogram shown in Fig. 4 (only shows Rio Grande). The shapes of these histograms are similar with maximum and minimal values for Rio Grande's buoy of 5.56 and -4.63 m, and the standard deviation and the 98th percentile of 0.55 m and 1.23 m, respectively.

The joint distribution of Hm0 and Tp, shown in Fig. 5, helps to understand how sets of simultaneous values of

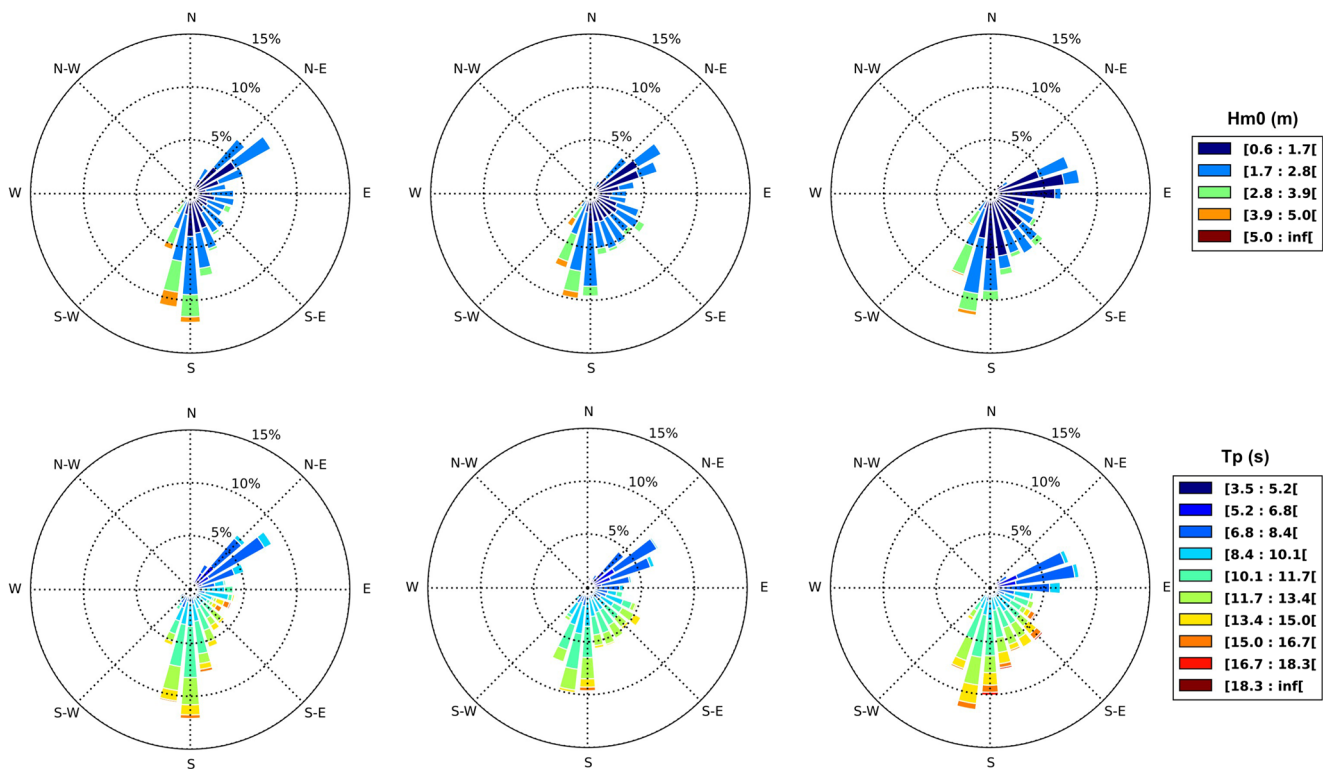
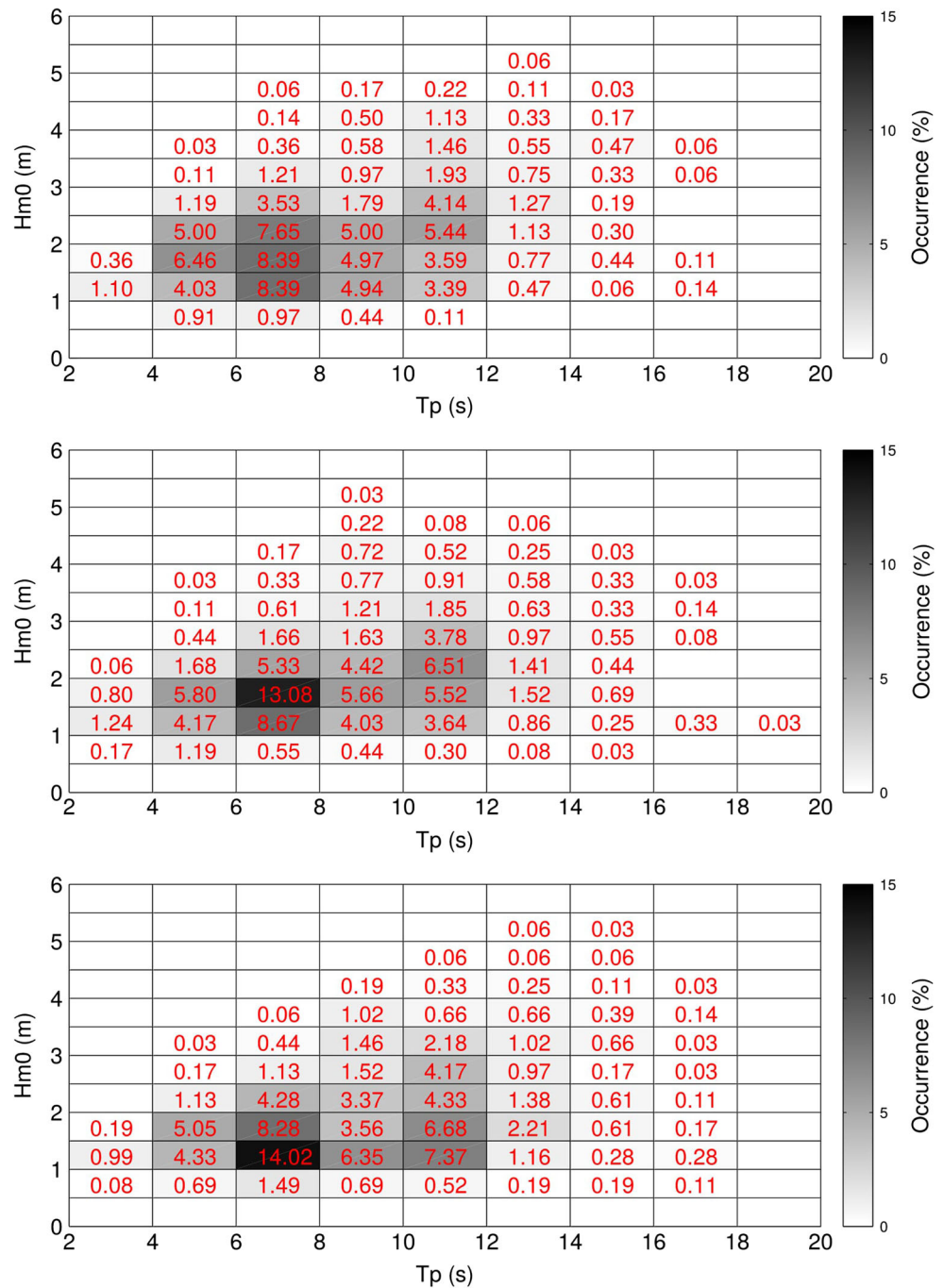


Fig. 3 Wave height roses (upper panel) and wave period roses (lower panel), from left to right: Rio Grande, Florianopolis and Santos. The direction represents where the waves comes from

Fig. 5 Joint distributions of the zero-moment wave height (H_{m0}) versus peak period (T_p). From top to bottom: Rio Grande, Florianopolis and Santos



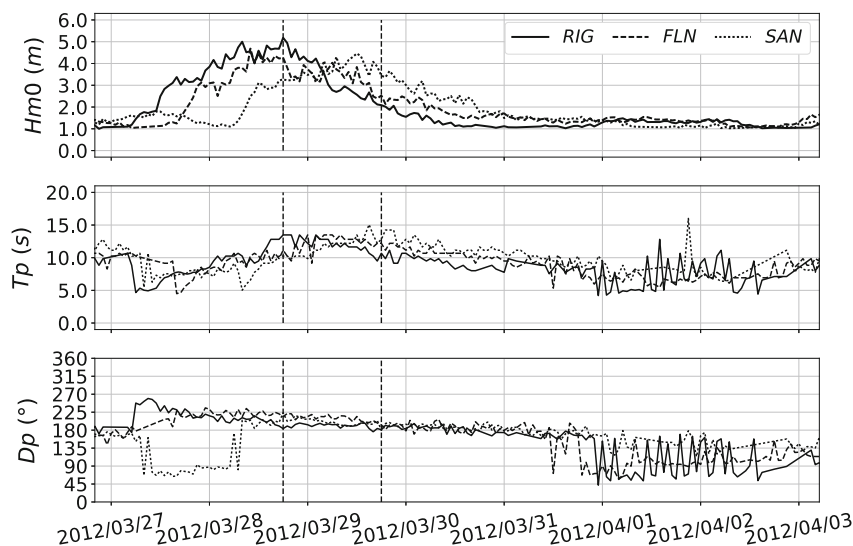
height and period, correspond to a given probability of occurrence. There is a clear dominance of peak period classes of 6–8 s and 10–12 s in all of the buoys. For Florianopolis’ and Santos’ buoys the modal classes of T_p between 6–8 s are more evident, with 12.95% of occurrence for H_{m0} classes of 1.5–2.0 m in Florianopolis’ and 14.02% for H_{m0} between 1.0–1.5 m in Santos’. It is important to stress that waves with large peak periods are more common in Florianopolis’ and Santos’ buoys, generally related with higher H_{m0} . Waves greater than 4 m occurred in 2.94% of the sea

states in Rio Grande. In Florianopolis and Santos, these percentages are equal to 2.1% and 1.18% respectively. On the other hand, T_p values that exceeded 14 s occurred in 2.36% (Rio Grande), 3.26% (Florianopolis) and 4.01% (Santos).

3.2 Spectral evolution

As shown in Fig. 1, the majority of the metocean buoys are within the subtropical zone, a region strongly affected by swell all year round. Campos Basin, located in the

Fig. 6 From top to bottom: zero-moment wave height (H_{m0}), peak period (T_p) and peak direction (D_p), spanning the period between the end of March and the beginning of April, 2012. The types of lines are related to different directional wave buoys, the solid line is the southernmost one and the dotted line the northernmost one. The arrival of the energetic waves as they propagate from south to north is evident, especially from the wave height time series (top panel). The dashed vertical lines depict two moments 24 h apart that are discussed in Fig. 7



Southeastern coast of Brazil (in the vicinity of 23S, 43W) and one of the most studied areas in the South Atlantic given its economic importance. As presented in Violante-Carvalho et al. (2004), around 75% of the 5800+ wave spectra recorded by a buoy deployed in deep water over a period of four years have two, three or more peaks with the low-frequency band containing most of the wave energy.

The frequent occurrence of multi-modal spectra is related to the typical meteorological conditions encountered there. The SAA, in general, generates waves at the higher frequency part of the wave spectrum. The lower frequency band of the spectrum, on the other hand, is associated with southerly waves generated by the passage of extratropical cyclones. The most typical trajectories of extratropical cyclones in the South Atlantic as well as the main cyclogenesis areas are presented in Rocha et al. (2004) and the references therein. This southerly swell is responsible for

most of the spectral energy in Campos Basin, and is ubiquitous along most of the Brazilian coast (Violante-Carvalho et al. 2004).

Swell attenuation propagating over large ocean basins is still poorly understood and therefore poorly predicted by numerical models. In the swell-dominated regions, the significant wave height tends to be overestimated due to a deficient representation of its energy attenuation. Measurements that quantify this energy decay are rare, especially because the instruments have to be aligned along which the waves propagate. One of the few experiments with in situ measurements was performed in the 1960s in the classical work by Snodgrass et al. (1966), with sensors covering most of the Pacific Ocean.

Since 1991, with the launch of ERS-1 and its successors ERS-2, ENVISAT and Sentinel1 carrying a Synthetic Aperture Radar (SAR), directional wave spectra are routinely

Fig. 7 Top panels display the energy spectra for the three southernmost buoys. Continuous line: Rio Grande, dashed line: Florianopolis and dotted line: Santos. The lower panels shows the wave direction (per frequency) measured at each buoy. The left panels correspond to the moment depicted by the left vertical dashed line in Fig. 6 (2012-03-28 at 18 h), while the right panels to the right vertical dashed line (2012-03-29 at 18 h)

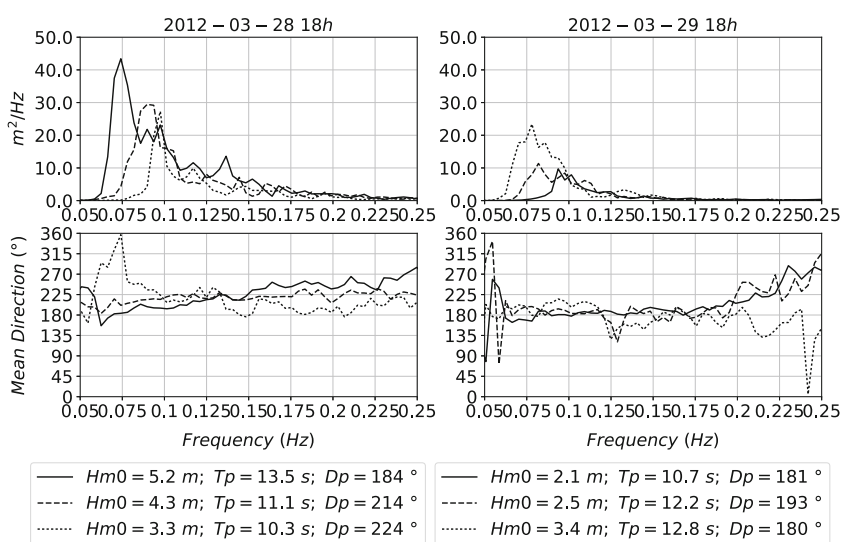


Table 4 Computational grids used in the simulations: $\Delta_{x,y}$ is the grid spacing in x and y , respectively. Lat_{in} and Lon_{in} are the initial latitude and longitude. Lat_{fi} and Lon_{fi} are the final latitude and longitude

Domain	$\Delta_{x,y}$	Lat_{in}	Lon_{in}	Lat_{fi}	Lon_{fi}
Grid 1	1.00°	−80°	−90°	60°	20°
Grid 2	0.25°	−45°	−65°	−5°	−10°

measured from space. In wave mode, an area of approximately 5 km by 5 km is mapped every second or so along the satellite track, yielding an enormous amount of directional information with global coverage. The extraction of wave spectra from SAR images is, however, a difficult task. The process of synthesizing a large antenna causes loss of information beyond a high frequency cut-off; therefore, the 2D wave spectra are limited in the azimuthal direction. Moreover, the transfer functions are complex and some degree of uncertainty is involved in the process (see the seminal paper by Hasselmann and Hasselmann 1991). Nonetheless, SAR onboard satellites are doubtless a powerful tool (Arduin et al. 2009).

The three southernmost metocean buoys (from south to north: Rio Grande, Florianopolis and Santos, depicted in Fig. 1) are particularly interesting for investigations on swell decay. Covering a distance of over 1000 km and being around 400 km apart of each other in roughly deep waters (200 m depth), they are aligned in one of the main directions in which long waves propagate towards lower latitudes. Figure 6 presents one energetic event on the 28th of March at 18 h when significant heights over 5 m and periods of

around 14 s were measured by the Rio Grande buoy, propagating at 200° (S/SW). A few hours later, they reach the other buoys, with the energy gradually reducing over the next two days.

The wave spectra at two moments represented by the vertical dashed lines in Fig. 6 are shown in Fig. 7. The left panels correspond to the moment when the wave energy peaked at the Rio Grande buoy (continuous line), with significant wave height of 5.2 m and peak period of 13.5 s. At this moment, the peak energy decreases northwards, while the peak frequency increases. At the right panels 24 h on, the direction of the waves at the three buoys are very close, with the northernmost buoy (Santos, dotted line) in turn measuring the longer and more energetic waves. In contrast, the energy and the peak frequency now decreases towards the south. This is a typical event of swell propagating roughly along the great circle where the three buoys are moored. Since the main generation areas are around one to two thousand kilometers away, these buoys are potentially interesting for investigations of swell evolution over comparatively shorter distances.

3.3 Comparison against wave model

3.3.1 Validation statistics

A wave hindcast for the 5 months of simultaneous buoy data was set using NCEP's Climate Forecast System Version 2 (CFSv2) wind and ice database. The hindcast was carried out using the third generation wind wave model WAVEWATCH III (hereinafter WW3) developed at the US National Centers for Environmental Prediction (NCEP).

Fig. 8 Time series of the zero-moment wave height (H_{m0}), peak period (T_p) and peak direction (D_p). WW3 (ST4 source term) vs. Rio Grande buoy data. The black dashed lines represent the moments of two freak wave events, detailed in Section 3.4

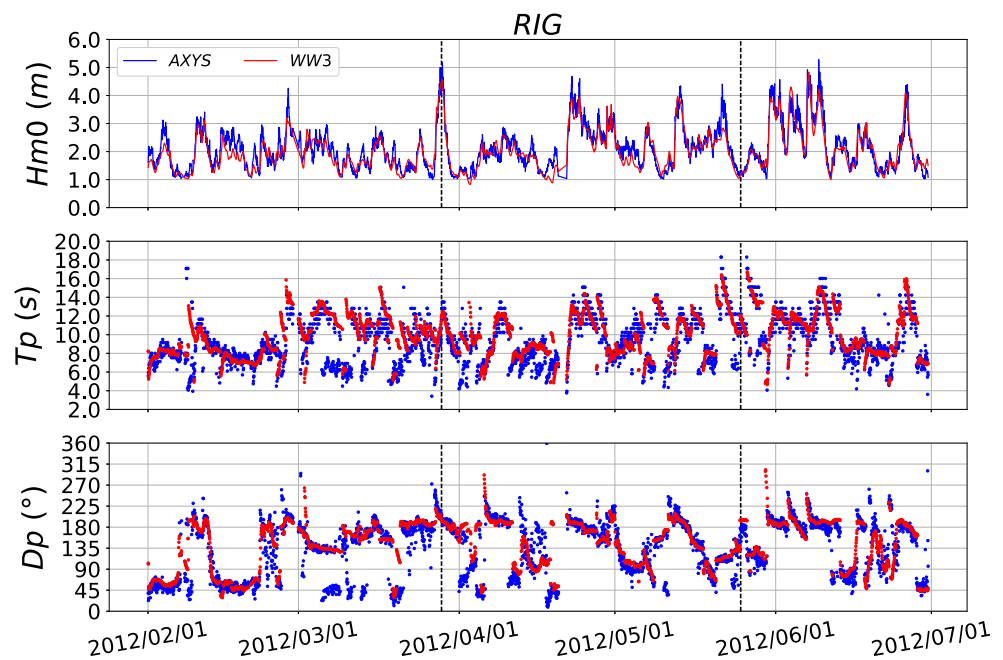
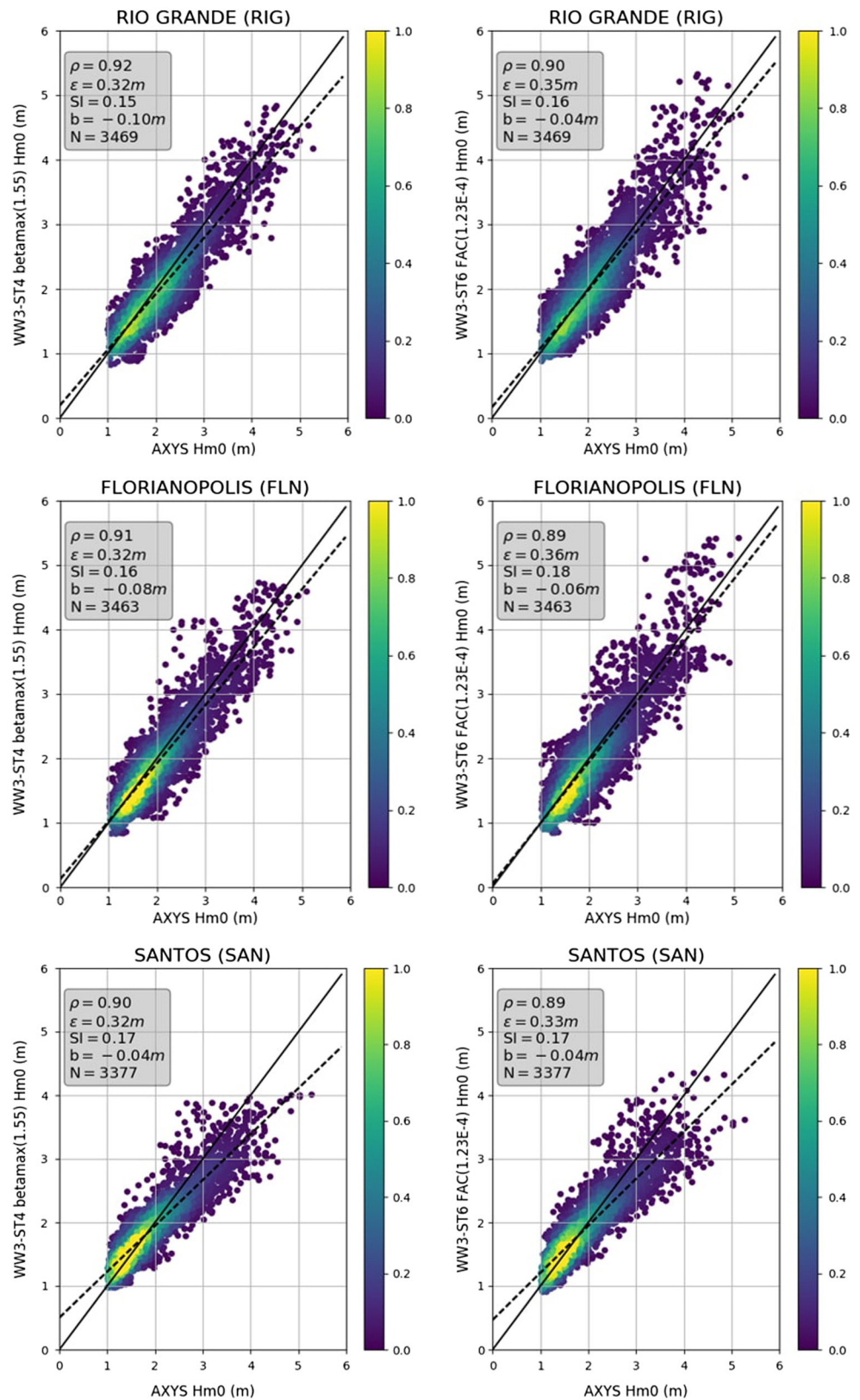


Fig. 9 Scatter probability plots (%) of the zero-moment wave height (H_{m0}) for the three southernmost buoys. The left panels correspond to the ST4 using $\beta_{max} = 1.55$. The right panels correspond to the ST6 using $FAC = 1.230E-4$. The legend contains the error statistics for correlation coefficient (ρ), root mean square error (ϵ), scatter index (SI), bias (b) and number of sample points (N)



WW3 solves the spectral action density balance equation for wavenumber-direction spectra. The governing equations of WW3 include refraction and frequency/wavenumber

shifting due to water depth and mean current variations. Parameterizations of physical processes (source terms) include wave growth and decay due to the actions of

wind, nonlinear resonant interactions, whitecapping, bottom friction, depth-induced breaking and scattering due to wave-bottom interactions (Tolman and Group 2014).

WW3 includes various source term packages (or physics): ST1 (or WAM3) (Komen et al. 1984; Snyder et al. 1981), ST2 (or TC96) (Tolman and Chalikov 1996), ST3 (WAM4+) (Bidlot et al. 2007; Janssen 1991), and recent implementations of ST4 (Ardhuin et al. 2010) and ST6 (or BYDRZ) (Zieger et al. 2015).

The ST4 parameterization is described by Ardhuin et al. (2010). This parameterization uses a positive part of the wind input that is taken from WAM4, with modified friction velocity to balance saturation-based dissipation. The dissipation term is defined as the sum of the saturation-based term, the cumulative breaking term, and the wave-turbulence interaction term (Ardhuin et al. 2009). Depending on the quality of the wind field, a wind-wave

growth parameter β_{max} can be adjusted. β_{max} is set to 1.55 for our implementation, as suggested by Ardhuin et al. (2010) (TEST405).

The ST6 or Babanin/Young/Donelan/Rogers/Zieger (BYDRZ) (Zieger et al. 2015) scheme implements observation-based physics for deep-water source/sink terms and includes negative wind input, whitecapping dissipation, and wave-turbulence interactions (swell dissipation). In the ST6, bulk adjustment to the wind field can be achieved by re-scaling the drag parameterization through the parameter FAC. This has a similar effect to the tuning variable β_{max} in ST4 source term package. In this work, the parameter FAC is adjusted to $FAC = 1.230E-4$, which performs well in the simulation using the CFSv2 wind.

The WW3 model was run for two different grids. Grid 1 covers the Atlantic Ocean and part of the Pacific Ocean and grid 2 covers the Southern Atlantic Ocean. Grid details can be found in Fig. 1 and Table 4.

Bathymetric data were obtained from ETOPO-1 database (Amante and Eakins 2009). The model has a resolution of 36 directions (10° angular bandwidth) and 35 logarithmically spaced frequencies, between 0.0377 Hz (26.5 s) and 0.9631 Hz (1.04 s).

Direct comparison between model simulations using WW3-ST4 package and the Rio Grande buoy data is presented in Fig. 8. In general, a good agreement can be noticed for wave height, peak periods and directions. Although the Hm0 results from WW3-ST4 are relatively close to the observed values, the largest wave heights were underestimated.

Furthermore, the WW3-ST4 model skill is evaluated against package ST6 using buoy data through the standard error metrics: Bias (b), Root Mean Square Error (ε), Scatter Index (SI) and Pearson's correlation coefficient (ρ). If x_i represents the measured values, y_i the simulated values and n the number of observations, the mentioned statistics are defined as follows:

$$Bias = \frac{\sum_{i=1}^n (x_i - y_i)}{n} \quad (2)$$

$$\varepsilon = \sqrt{\frac{\sum_{i=1}^n (x_i - y_i)^2}{n}} \quad (3)$$

$$SI = \frac{\varepsilon}{\bar{y}} \quad (4)$$

$$\rho = \frac{\sum_{i=1}^n (x_i - \bar{x})(y_i - \bar{y})}{\sqrt{(\sum_{i=1}^n (x_i - \bar{x})^2 \sum_{i=1}^n (y_i - \bar{y})^2)}} \quad (5)$$

where the overbar denotes average values.

Scatter density plots of the zero-moment wave height (Hm0) are shown in Fig. 9 considering the ST4 and ST6 packages. In addition, statistics were computed for the zero

Table 5 Bias (b), root mean square error (ε), scatter index (SI) and correlation coefficient (ρ) for the correlations between wave parameters given by the buoys and those given by WW3, considering the ST4 and ST6 packages

Index	Wave Param.	RIG	FLN	SAN
b - ST4	Hm0 (m)	-0.10	-0.08	-0.04
	Tp (s)	0.59	0.57	0.53
	Dp (°)	10.58	11.74	9.59
ε - ST4	Hm0 (m)	0.32	0.32	0.32
	Tp (s)	2.03	2.00	2.03
	Dp (°)	43.63	51.32	34.02
SI - ST4	Hm0	0.15	0.16	0.17
	Tp	0.22	0.21	0.20
	Dp	0.33	0.37	0.24
ρ - ST4	Hm0	0.92	0.91	0.90
	Tp	0.68	0.71	0.69
	Dp	0.71	0.62	0.75
b - ST6	Hm0 (m)	-0.04	-0.06	-0.04
	Tp (s)	0.67	0.70	0.72
	Dp (°)	10.30	11.84	9.22
ε - ST6	Hm0 (m)	0.35	0.36	0.33
	Tp (s)	2.12	2.10	2.05
	Dp (°)	43.60	52.77	35.51
SI - ST6	Hm0	0.16	0.18	0.17
	Tp	0.23	0.22	0.21
	Dp	0.33	0.39	0.25
ρ - ST6	Hm0	0.90	0.89	0.89
	Tp	0.65	0.69	0.70
	Dp	0.71	0.61	0.72

moment wave height, peak wave period and mean wave direction corresponding to the peak period. The values of the statistical parameters are displayed in Table 5.

It can be noticed that the ST4 and ST6 source terms are fairly consistent in overall error statistics. In terms of H_{m0} , the scatter index values (or relative error) are less than 0.2 for both runs (ST4 and ST6). The ε is 0.32 m for ST4 on the three buoys. For ST6, the ε varies from 0.33 m at Santos buoy to 0.36 m at Florianopolis buoy. Both parameterizations show a negative bias, but the bias is a little lower in the ST6 runs. However, in terms of ε and SI, the wave heights are better with the ST4 source term packages.

Regarding wave periods, results are better with ST4, while for directions ST6 gives slightly better results. From Table 5, ST4 provides slightly better results than the ST6

source term. Therefore, the next considerations will be made with the ST4 source term.

3.3.2 Swell arrival

The knowledge of swell arrival time plays an important role for many offshore activities and navigation. The evaluation of this arrival time in numerical models is an important task which has been studied to improve this physics in wave models. Jiang et al. (2016) shows that models can be 20 h early or 20 h late compared with observed data, but usually predicts an early arrival of swell, about 4 h on average, in a distance of thousand of kilometers.

To make considerations about swell arrival, a time window for waves with peak period greater than 10 s was chosen.

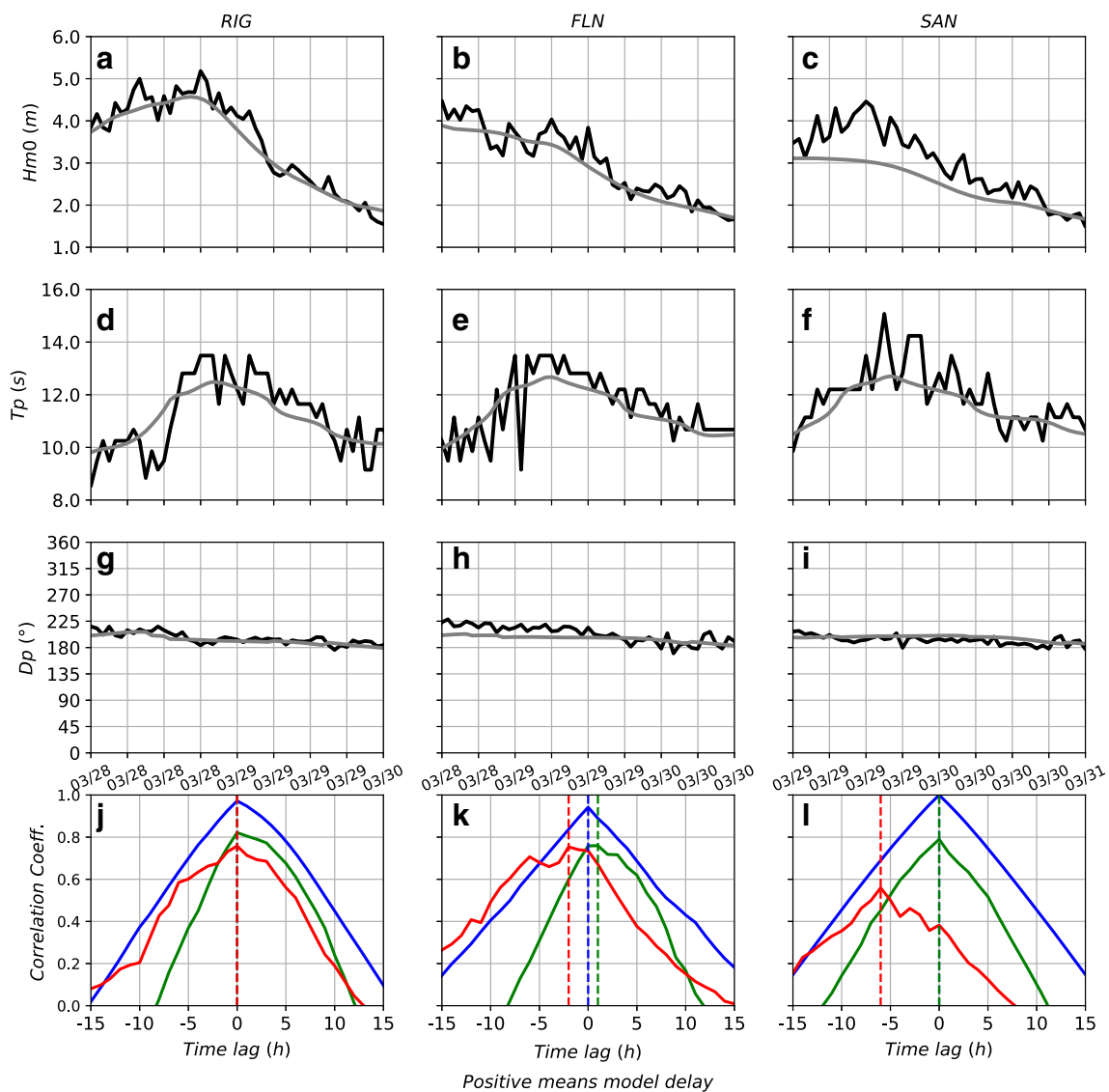


Fig. 10 a–c Wave height, d–f peak period, g–i peak directions (Buoy - black; Model - gray), and j–l arrival time differences of the same swell event in Rio Grande, Florianopolis and Santos buoys (H_{m0} - blue; T_p -

green and D_p - red). Positive lag means model delay (i.e. swell arrives early in the buoy compared with the model)

Figure 10 shows H_m0 , T_p and D_p in the first three rows, respectively, and the last row presents arrival time differences (correlation coefficient and time lag - positive lag means model delay) for each wave parameter (H_m0 -blue; T_p -green and D_p -red). Each column represents one buoy.

In general, it is possible to verify that H_m0 and T_p were well represented by the model, that is, the time lag equals zero. However, there is a clear delay in the peak direction in the buoys in Florianopolis and Santos. In Florianopolis the model shows a time lag of minus 5 h (model is early) and minus 6 h for Santos.

3.4 Comparison against radar altimeters

Radar altimeters onboard satellites are also capable of providing high-quality wave heights (H_m0), of which the typical accuracy in terms of ε is about 0.2 m (e.g., Zieger et al. 2009). The calibration and validation of altimeter-observed H_m0 , however, were mainly achieved in the North Hemisphere, especially the area close to the US coastline (see Fig. 1 of Zieger et al. 2009 for example). With the network of wave buoys described herein, we are able to evaluate H_m0 (and wind speed U_{10}) measurements from altimeters in the south Atlantic Ocean, particularly along the Brazilian

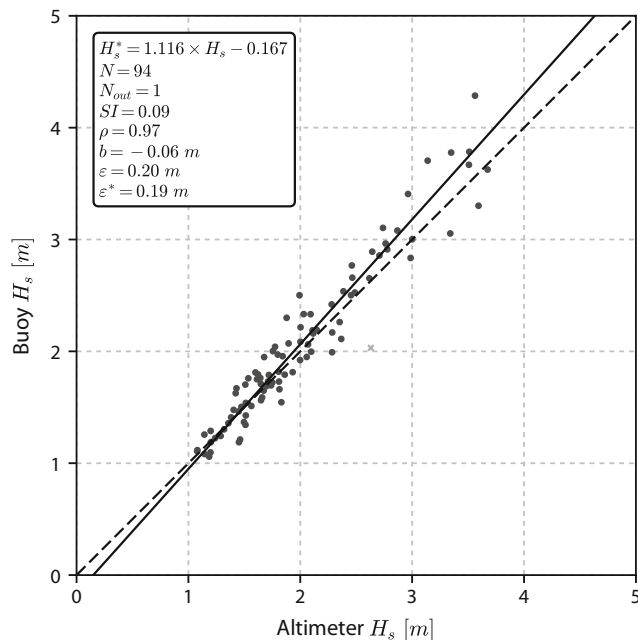


Fig. 11 Comparison of wave height (H_m0) observed by altimeters (horizontal axis) and buoys (vertical axis). Collocated measurements are considered within 50-km radius and 30-min temporal separation. The solid line represents the reduced-major-axis (RMA) fit and the dashed line is the 1:1 line. Error statistics for scatter index (SI), correlation coefficient (ρ), bias (b), root mean square error (ε), and number N of sample points are given in the inset, with outliers N_{out} (detected by robust regression) labeled with gray crosses. The term ε^* signifies the root mean square error after the RMA correction. For the technical details, please refer to Zieger et al. (2009) and Liu et al. (2016a)

coast. An example of such application can be found in Fig. 11, where H_m0 from both altimeters and the three buoys (namely RIG, FLN, SAN) were collocated and compared. The widely-accepted criteria, i.e., 50 km for spatial separation and 30 min for time separation, were adopted here. The altimeter data were sourced from the fully calibrated and validated multi-platform dataset established by Zieger et al. (2009) and then later extended by Liu et al. (2016a). Three altimeters, including *Jason-2*, *CryoSat-2* and *HY-2*, were selected for the specific five months we concern (Feb - Jun 2012). Besides, H_m0 from these three altimeters has been corrected following Liu et al. (2016a) (see Appendix A).

Examination of Fig. 11 shows that a total of 94 altimeter collocations were found. Relative to in situ buoy measurements, altimeter-observed H_m0 is only 6 cm biased low, with a minor root mean square error (ε) of 0.2 m. The correlation coefficient (ρ) is as high as 0.97, and the scatter index (SI) is less than 0.1. The excellent agreement between buoy data and altimeter records as seen here are consistent with the patterns when altimeter-recorded H_m0 was compared against buoys in the North Atlantic (e.g. Zieger et al. 2009, Liu et al. 2016a) and the Arctic Ocean (e.g., Liu et al. 2016b). With a long-term operation of this buoy network, a detailed examination of altimeter-derived wave climate (e.g. Young et al. 2011) in this local region will become feasible in the future.

3.5 Freak waves

The individual wave height probability distribution, associated to a specific sea state, is one of the key sea features for determining the occurrence of a rogue wave. If a single wave has an abnormal and unexpected wave height,

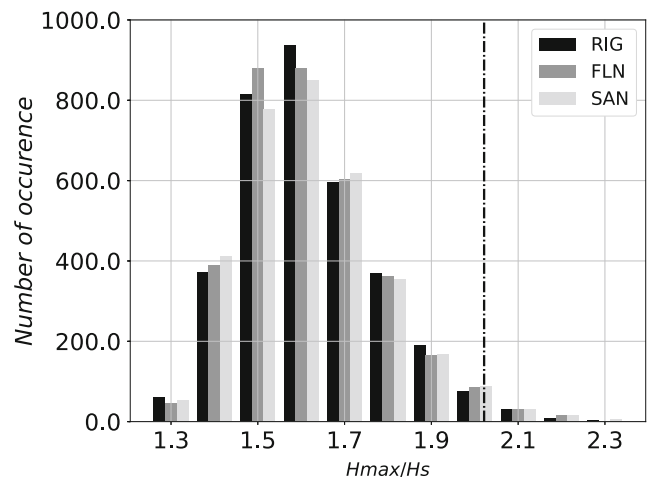


Fig. 12 Histogram for the ratio between maximum wave height (H_{max}) and significant wave height (H_s). The dashed line represents the 2.0 limit

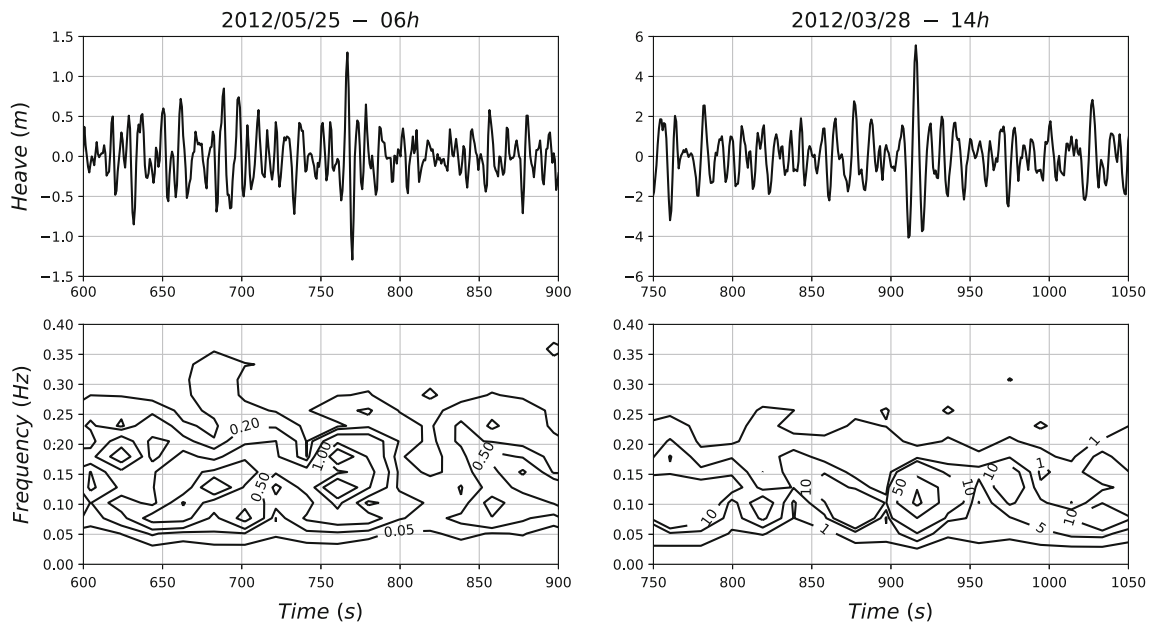


Fig. 13 Upper panel (heave time series), lower panel (its spectrogram). Left panel: good weather condition; right panel: stormy sea condition

this individual wave is defined frequently as a rogue or freak wave, although the exact definition of such waves can vary substantially. Many variables of the sea state have been directly related to the occurrence of the abnormal high waves, namely: wave steepness, spectral bandwidth, wave directionality, spectral tail, wind forcing (Babanin and Rogers 2014), wave age and horizontal wave asymmetry (Kharif et al. 2009). Some authors consider the higher possible wave height expected as a linear superposition, in a wave storm with a long enough duration, as twice H_s , being the more usual definition. Others define freak wave as being the individual wave height equal to or greater than $2.2H_s$, which cannot be explained as a simple superposition of linear waves (Babanin and Rogers 2014).

Pinho et al. (2004) analyzed data from a pitch and roll buoy moored in Campos Basin, off Rio de Janeiro from 1991 to 1995, finding occurrences of freak waves in both stormy and calm conditions. In another study in the south atlantic, Candella (2016) analyzed the characteristics of freak waves using the same three buoys used in this work (RIG, FLN and SAN). Applying parameters such as crest amplification index and lower limit to significant wave height, only 7 “true” freak waves were found.

To assess the distribution of H_{max}/H_s values, a histogram for these relationship is shown in Fig. 12. It is observed that the highest occurrence lies around 1.6 m, decreasing practically to zero for values greater than 2.0.

Approximately 2.88% of the 3469 cases (i.e., 100 cases) reached the relation $H_{max}/H_s > 2$ for Rio Grande. For Florianopolis and Santos, the number of cases that reached the above relation is equal to 109 out of 3463 (3.15%) and 116 out of 3377 (3.44%), respectively.

Figure 13 presents the spectrograms for two heave time series referring to Rio Grande’s buoy. In the left panel (good weather condition) at the position of the freak wave, the energy is broadly spread in the high frequency portion of the spectrum, which is, according to Liu et al. (1979), a freak wave characteristic. Whilst in the other case, in the stormy sea condition (right panel), the energy at the instant of occurrence of the freak wave is concentrated around the peak frequency. The time series in the left panel is the one with the maximum H_{max}/H_s relationship in our record (i.e., 2.4) while in the right panel is the one with the highest significant wave height. These examples illustrate the occurrence of extreme waves in a region dominated by swell with multi-peaked spectra.

4 Conclusions

Several simultaneous directional buoy measurements spanning a period of roughly 5 months acquired in deep water are employed for the assessment of the wave characteristics in the southernmost coast of Brazil. The three ones selected in the analysis are part of an array of 10 metocean buoys along the Brazilian coast, within the PNBOIA program currently in operation. They were selected because of the simultaneity of measurements without significant gaps in the data and over one of the most energetic areas of the South Atlantic, in the vicinity of the Brazil-Malvinas Confluence Zone and in the frequent pathways of extratropical cyclones. The South Atlantic is well known for the scarcity of in situ measurements; therefore, the dataset here presented is the result of a collaborative effort to establish a network of metocean buoys.

Our goal in this paper is to present several results aiming to characterise the wind waves, through statistical and spectral analysis. The mean bulk wave parameters show that the significant wave height is around 2 m, with a slight tendency to decrease northwards. Peak period, on the other hand, presents a mean value of about 9.5 s, increasing northwards. All three buoys present bimodal sea state characteristics. The wave direction is mainly from SW, related to longer waves, and from NE related to short period waves. The joint distribution of H_{m0} versus T_p shows that the most recurrent waves have periods of 6–8 s and 10–12 s with H_{m0} of 1–2 m. The spectral evolution analysis illustrates an example where there is a time gap of around 12 h during the dispersive arrival of a south-southwesterly swell propagating along the aligned buoys. Statistical assessment of numerical wave model was performed employing different source terms, namely ST4 and ST6 in WW3 forced by CFSv2 winds, with both in good agreement with buoy data. ST6 presented smaller bias, while for the other statistical terms ST4 was in better agreement with the buoy data. Comparison against altimeters also shows good agreement. Some freak wave events are also indicated, and the main circumstances in which they occurred are discussed.

Although the main focus is the analysis of wave data, the meteocean buoys have a variety of instruments. Several parameters are available at the web page, among them air and water temperature, wind speed and direction, current profile in the upper 50 m with high spatial and temporal resolution as well as wave information. The data is freely downloadable to the scientific community. For our best knowledge, for the western part of the South Atlantic, currently, there is no other meteocean database as comprehensive as the one here described.

Acknowledgements We would like to thank the Hydrographic Center of the Brazilian Navy (CHM). Alex V. Babanin acknowledges the grant 88881.062163/2014-01 from the Coordination for the Improvement of Higher Education Personnel (CAPES) as a Special Visiting Researcher from the Brazilian Science Without Borders program.

Appendix A

Altimeter data

In this article, H_{m0} data from three altimeters, namely *Jason-2*, *CryoSat-2* and *HY-2*, have been selected to

inter-compare with buoy wave measurements. The original 1-Hz altimeter records were quality-controlled, calibrated and validated in Liu et al. (2016a). Calibrations of these wave data are summarized in the Table 6.

References

- Amante C, Eakins B (2009) Etopo1 1 arc-minute global relief model: Procedures, data sources and analysis. NOAA Technical Memorandum NESDIS NGDC-24
- Ardhuin F, Chapron B, Collard F (2009) Observation of swell dissipation across oceans. *Geophys Res Lett* 36:1–5
- Ardhuin F, Rogers E, Babanin AV, Filipot J-F, Magne R, Roland A, van der Westhuysen A, Queffelec P, Lefevre J-M, Aouf L, Collard F (2010) Semiempirical dissipation source functions for ocean waves. Part i: definition, calibration, and validation. *J Phys Oceanogr* 40(9):1917–1941
- Babanin AV, Rogers WE (2014) Rogue waves in the ocean, generation and limiters. In: Proceedings of the fifth indian national conference on harbour and ocean engineering (INCHOE)
- Badulin SI, Babanin AV, Zakharov VE, Resio D (2007) Weakly turbulent laws of wind-wave growth. *J Fluid Mech* 591:339–378
- Bidlot J-R, Janssen P, Abdalla S (2007) A revised formulation of ocean wave dissipation and its model impact. Technical Memorandum 27
- Candella RN (2016) Rogue waves off the South/Southeastern Brazilian coast. *Nat Hazards* 83:1–22
- Chawla A, Spindler DM, Tolman HL (2013) Validation of a thirty year wave hindcast using the climate forecast system reanalysis winds. *Ocean Modell* 70:189–206
- Cuchiara DC, Fernandes EH, Strauch JC, Winterwerp JC, Calliari LJ (2009) Determination of the wave climate for the Southern Brazilian shelf. *Cont Shelf Res* 29:545–555
- Hasselmann K, Hasselmann S (1991) On the nonlinear mapping of an ocean wave spectrum into a synthetic aperture radar image spectrum and its inversion. *J Geophys Res Oceans* 96(C6):10713–10729
- Hemer MA, Church JA, Hunter JR (2009) Variability and trends in the directional wave climate of the Southern Hemisphere. *Int J Climatol* 30(4):475–491
- Janssen PAEM (1991) Quasi-linear theory of wind-wave generation applied to wave forecasting. *J Phys Oceanogr* 21(11):1631–1642
- Jiang H, Babanin AV, Chen G (2016) Event-based validation of swell arrival time. *J Phys Oceanogr* 46:3563–3569
- Kharif C, Pelinovsky E (2003) Physical mechanisms of the rogue wave phenomenon. *Eur J Mec - B/Fluids* 22(6):603–634
- Kharif C, Pelinovsky E, Slunyaev A (2009) *Rogue waves in the ocean*. Springer, Berlin
- Komen GJ, Hasselmann K, Hasselmann K (1984) On the existence of a fully developed wind-sea spectrum. *J Phys Oceanogr* 14(8):1271–1285
- Liu PC (2007) A chronology of freak wave encounters. *Geofizika* 24(1):57–70

Table 6 Altimeter data and calibration used in Section 3.4 for the period over the five months from Feb to Jun 2012. The reader is referred to Table 3 of Liu et al. (2016a) for more details

Altimeter	H_{m0} calibration
<i>Jason-2</i>	$H_{m0}^* = 1.019 \times H_{m0} - 0.050$
<i>CryoSat-2</i>	$H_{m0}^* = \begin{cases} 0.836 \times H_{m0} + 0.157 & H_{m0} \leq 1.853 \text{ m} \\ 1.001 \times H_{m0} - 0.149 & H_{m0} > 1.853 \text{ m} \end{cases}$
<i>HY-2</i>	$H_{m0}^* = \begin{cases} 1.003 \times H_{m0} + 0.287 & H_{m0} \leq 3.504 \text{ m} \\ 0.040 \times H_{m0}^2 + 0.838 \cdot H_{m0} + 0.376 & H_{m0} > 3.504 \text{ m} \end{cases}$

- Liu WT, Katsaros KB, Businger JA (1979) Bulk parameterization of air-sea exchanges of heat and water vapor including the molecular constraints at the interface. *J Atmos Sci* 36(9):1722–1735
- Liu Q, Babanin AV, Guan C, Zieger S, Sun J, Jia Y (2016a) Calibration and validation of HY-2 altimeter wave height. *J Atmos Ocean Technol* 33(5):919–936
- Liu Q, Babanin AV, Zieger S, Young IR, Guan C (2016b) Wind and wave climate in the arctic ocean as observed by altimeters. *J Clim* 29(22):7957–7975
- Parise C, Farina L (2012) Ocean wave modes in the South Atlantic by a short-scale simulation. *Tellus A Dyn Meteorol Oceanogr* 64(1):17362
- Pianca C, Mazzini PLF, Siegle E (2010) Brazilian offshore wave climate based on nww3 reanalysis. *Braz J Oceanogr* 58:53–70
- Pinho UF, Liu PC, Parente CE (2004) Freak waves at campos basin, Brazil. *Geofizika* 21:53–67
- Rapizo H, Babanin AV, Schulz E, Hemer MA, Durrant TH (2015) Observation of wind-waves from a moored buoy in the Southern Ocean. *Ocean Dyn* 65(9):1275–1288
- Rocha RP, Sugahara S, Silveira RB (2004) Sea waves generated by extratropical cyclones in the South Atlantic ocean: Hindcast and validation against altimeter data. *Weather Forecast* 19(2):398–410
- Snodgrass FE, Groves GW, Hasselmann KF, Miller GR, Munk WH, Powers WH (1966) Propagation of ocean swell across the pacific. *Philos Trans R Soc A Math Phys Eng Sci* 259(1103):431–497
- Snyder RL, Dobson FW, Elliott JA, Long RB (1981) Array measurements of atmospheric pressure fluctuations above surface gravity waves. *J Fluid Mech* 102:1–59
- Souza MHS, Parente CE (1988) Wave climate off Rio de Janeiro. *Coastal Eng Proc* 1(21):261–269
- Tolman HL, Chalikov D (1996) Source terms in a third-generation wind wave model. *J Phys Oceanogr* 26(11):2497–2518
- Tolman H, Group (2014) User manual and system documentation of wavewatch iii version 4.18. NOAA/NWS/NCEP/MMAB Technical Note 316, 282pp
- Tucker M, Pitt E (2001) Waves in ocean engineering. Elsevier Ocean Engineering Book Series, vol 5
- Violante-Carvalho N, Ocampo-Torres FJ, Robinson IS (2004) Buoy observations of the influence of swell on wind waves in the open ocean. *Appl Ocean Res* 26(1–2):49–60
- Welch PD (1967) The use of fast fourier transform for the estimation of power spectra: a method based on time averaging over short, modified periodograms. *IEEE Trans Audio Electroacoust* 15:70–73
- Young IR, Zieger S, Babanin AV (2011) Global trends in wind speed and wave height. *Science* 332:451–455
- Zieger S, Vinoth J, Young IR (2009) Joint calibration of multiplatform altimeter measurements of wind speed and wave height over the past 20 Years. *J Atmos Ocean Technol* 26:2549–2564
- Zieger S, Babanin AV, Rogers WE, Young IR (2015) Observation-based source terms in the third-generation wave model {WAVEWATCH}. *Ocean Model* 96(Part 1):2–25. Waves and coastal, regional and global processes